Electronic Supplementary Material (ESI) for Energy & Environmental Science.

Electronic Supplementary Information

Operando X-ray spectroscopic tracking of self-reconstruction for anchored nanoparticles as high-performance electrocatalysts towards oxygen evolution

Sanzhao Song[a,b,‡], Jing Zhou[a,‡], Xiaozhi Su[a], Yu Wang[a,*], Jiong Li[a], Linjuan Zhang[a], Guoping Xiao[a], Chengzhi Guan[a], Renduo Liu[a], Shuguang Chen[a], Hong-Ji Lin[c], Shuo Zhang[a,*] & Jian-Qiang Wang[a,b,*]

[a] Shanghai Institute of Applied Physics, Chinese Academy of Sciences 201800, Shanghai, China.

[b] University of Chinese Academy of Sciences 100049, Beijing, China.

[c] National Synchrotron Radiation Research Center 30076, Hsinchu, Taiwan, China.

‡ These authors contributed equally to this work.

Experimental Section

Material Synthesis

The $LaCoO_{3-\delta}$ (LCO) was synthesized using the molten salt method. The metal precursors La_2O_3 (99.9%, Alfa Aesar) and Co_3O_4 (99.9%, Alfa Aesar) were used as-received. The alkali metal chloride NaCl (Aladdin, 99.9%) and KCl (Aladdin, 99.9%) were dried at 100°C for 24 h. The eutectic mixture, with the melting point of 657 °C, was obtained by mixing the dried NaCl and KCl in an agate mortar at a molar ratio of 1:1. The weight ratio between mixed oxide and molten salt was 1:2. The syntheses were carried out in alumina crucibles placed into a tube furnace and heated in 850 °C for 5 h. After cooling, the soluble compounds of the reaction mixtures were dissolved in distilled water and the solid product was centrifuged and washed repeatedly. Finally, the sample was dried in vacuum overnight at 60 °C to remove the remaining water. Then the powders of LCO were transferred into an alumina boat, and reduced in a tube furnace at 700 °C for 3 h in a flow of 5% H_2/Ar. The reduced powders were denoted as LCO-700. Co nanoparticles (NPs) with size of 30 nm (99.9% metals basis, Alfa Aesar) was also used as received.

Physicochemical characterizations

Scanning electron microscopy (SEM) was performed by using a ZEISS Merlin Compact Field Emission Scanning Electron Microscope with an acceleration voltage of 5 kV. Transmission electron microscopy (TEM) equipped with an Energy-dispersive X-ray Spectrum (EDX) was taken from a Tecani-G2 T20 and F20 operating at an acceleration voltage of 200 kV.

The BET specific surface areas of the prepared catalysts were determined by adsorption–desorption of nitrogen at liquid nitrogen temperature, using a Micromeritics TriStar 3000 equipment. Sample degassing was carried out at 300 °C prior to acquiring the adsorption isotherm.

H_2-TPR measurements

TPR profiles were obtained by AutoChem HP 2950 apparatus from Micromeritics. Approximate 50 mg of freshly calcined catalyst was placed in a U-shape quartz tube. The sample (50 mg) was pretreated at 500 °C for 2 h in He and cooled to 25 °C in flowing He. TPR experiments were carried out in 5 vol.% H_2/Ar flowing at 40 mL min^{-1} with a ramping rate of 10 °C min^{-1} to a final temperature of 850 °C. The H_2 consumption was monitored using a thermal conductivity detector (TCD).

Electrochemical measurements of OER activities

RHE calibration of the Ag/AgCl reference electrode in 0.1 M KOH was also tested. The calibration was performed in the high purity hydrogen saturated electrolyte with a Pt wire as the working electrode. CVs were run at a scan rate of 1 mV s^{-1}, and the average of the two potentials at which the current crossed zero was taken to be the thermodynamic potential for the hydrogen electrode reactions.

The electrolyte was 0.1-M KOH aqueous solution (99.99% metal purity,), which was saturated with O_2 for 30 min prior to each test and maintained under O_2 atmosphere throughout. Then Mettler-FE28-standard (Mettler-Toledo Instruments (shanghai) Co., Ltd.) was used to measure the pH of KOH solution, which is about 12.8.

The long-term test was obtained after the LCF-700 was completely activated and stabilized, then chronopotentiometric measurement at j = 10 mA cm^{-2} was performed.

The XRD and TEM measurements of the activated catalyst were performed by the following method: First, we dropped the ink of catalyst on the carbon paper and dried in the air for 1 hour. Next, we used it for electrochemical measurement. After that the XRD and TEM characterization was performed.

Electrochemical calculation method

The values of mass activity (A g^{-1}) were calculated from the oxide catalyst loading m (0.245 mg cm^{-2}) and the measured current density j (mA cm^{-2}) at η = 293 mV by the following equation:

$$\text{mass activity} = j/\text{m}.$$

The values of specific activity (mA cm^{-2}) were calculated from the BET surface area S_{BET} (m^2 g^{-1}), oxide catalyst loading m, and the measured current density j (mA cm^{-2}) at η by the following equation:

$$\text{specific activity} = j / (10\times\text{m}\times S_{BET}).$$

EXAFS fitting

The following equation was used in EXAFS fitting:

$$\chi(k) = \sum_j \frac{N_j S_0^2 F_j(k)}{k R_j^2} \exp\,[-2k^2\sigma_j^2] \exp\,[\frac{-2R_j}{\lambda(k)}] \sin\,[2kR_j + \phi_j(k)]$$

N_j is the number of neighbors in the j^{th} atomic shell. S_0^2 is the amplitude reduction factor. $F_j(k)$ is the effective curved-wave backscattering amplitude. R_j is the distance between the X-ray absorbing central atom and the atoms in the j^{th} atomic shell (backscatterer). λ is the mean free path in Å. $\phi_j(k)$ is the phase shift (including the phase shift for each shell and the total central atom phase shift). σ_j is the Debye-Waller parameter of the j^{th} atomic shell (variation of distances around the average R_j). The functions $F_j(k)$, λ and $\phi_j(k)$ were calculated with the *ab initio* code FEFF8.2.

The coordination numbers of model samples (Co foil and Fe foil) were fixed as the nominal values. The obtained S_0^2 of Co foil was 0.73, and was fixed in the subsequent fitting of Co *K*-edge data for LCF samples. The obtained S_0^2 of Fe foil was 0.70. For the simulation at the Co *K*-edge and

Fe *K*-edge of LCF, the theoretical models used for the EXAFS fitting were generated from the $LaCoO_3$ structure (Co-O, Co-La and Co-Co path) and $LaFeO_3$ structure (Fe-O path). The cobalt and iron structure (Co-Co and Fe-Fe path) were used for the fittings on the metallic cobalt and iron of samples. For the analysis of *operando* EXAFS measurements at the Co *K*-edge, the coordinates were taken from the metallic cobalt (Co-Co path) and CoOOH structure (Co-O and Co-Co path). For the simulation at the *operando* Fe *K*-edge EXAFS, metallic iron (Fe-Fe path) and FeOOH structure (Fe-O path) were used for the fittings. The obtained parameters were listed in Table S1, S2, S4 and S5.

Co $L_{2,3}$-edge XAS fitting

To further verify the electronic configurations of Co, we performed XAS measurements at Co $L_{2,3}$-edge. All spectra were collected at room temperature at the 11A beamline of the National Synchrotron Radiation Research Center (NSRRC) in Taiwan using total-electron-yield (TEY) model. CoO single crystals were measured simultaneously to serve as energy references for the Co $L_{2,3}$-edge.

The line shape of XAS at TM $L_{2,3}$-edge strongly depends on the multiplet structure given by the TM 3d-3d and 2p-3d Coulomb and exchange interactions, as well as by the local crystal fields and the hybridization with the O 2p ligands. This makes this technique extremely sensitive to valence states of the ions. Here we used Co metal, CoO, $LaCoO_3$ and $BaCoO_3$ as the references of Co^0, Co^{2+}, Co^{3+} and Co^{4+}, respectively. We have made composite spectra by linear combination of the reference spectra and compare to the experimental spectra. The ratio of different reference spectra is carefully adjusted to get the best fitting of the experimental spectra. By this procedure, the proportion of Co, Co^{2+}, Co^{3+} and Co^{4+} in the samples could be estimated.

Supporting Figures

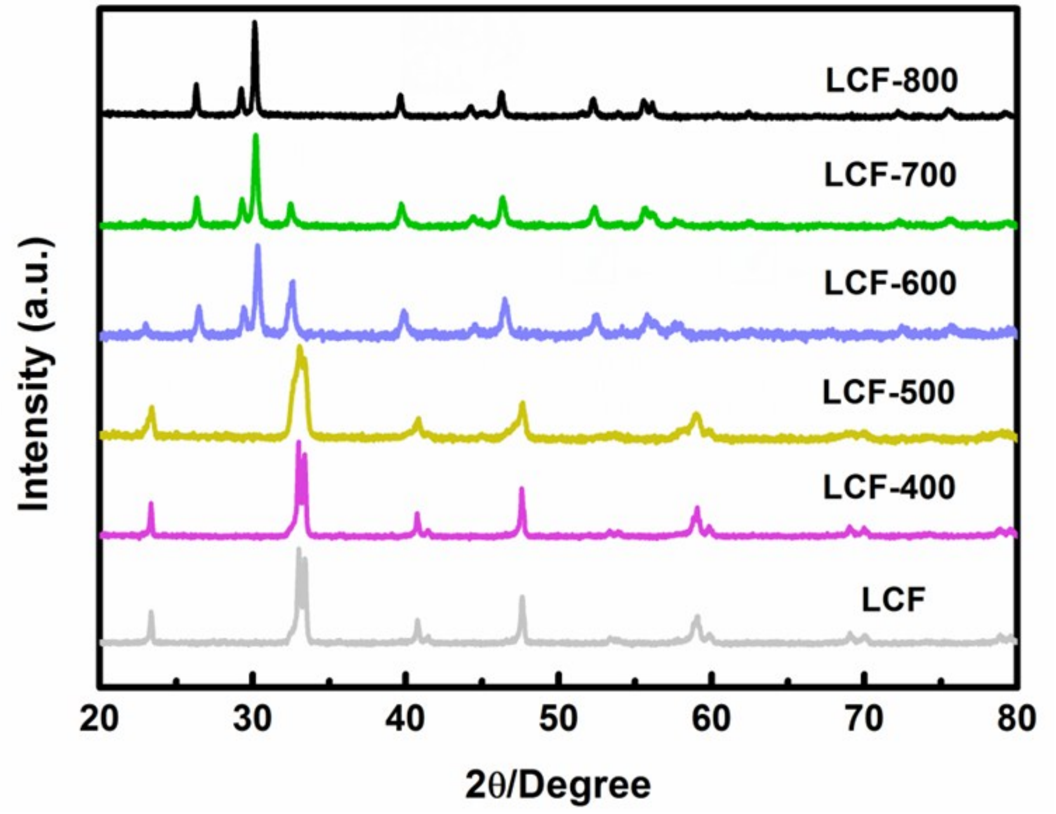

Fig. S1 The XRD patterns of $LaCo_{0.8}Fe_{0.2}O_{3-\delta}$ (LCF) and the samples reduced at different temperatures.

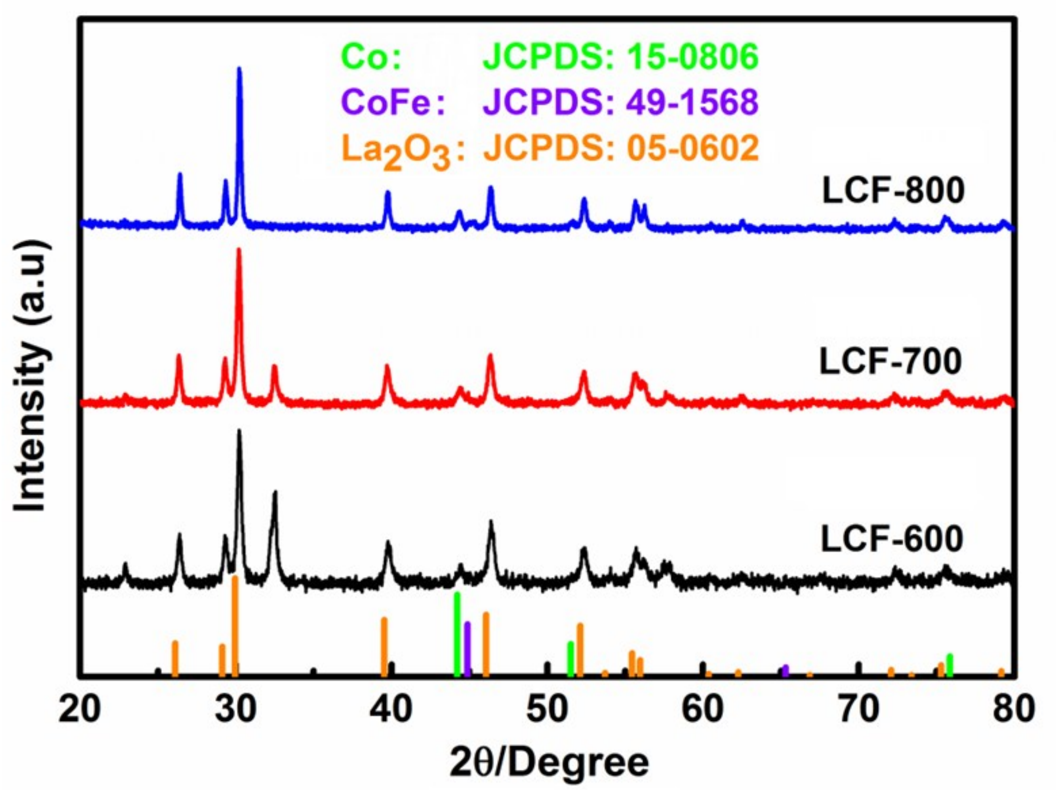

Fig. S2 The XRD patterns of LCF-600, LCF-700 and LCF-800.

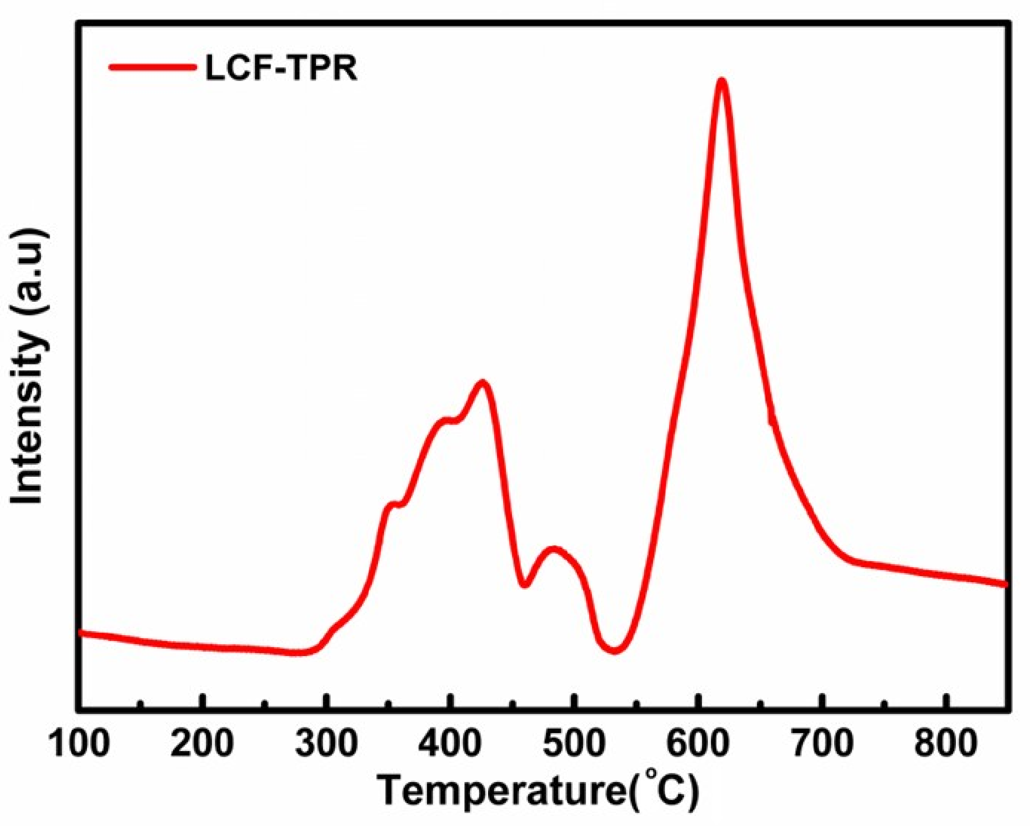

Fig. S3 Temperature program reduction (TPR) measurement for the LCF.

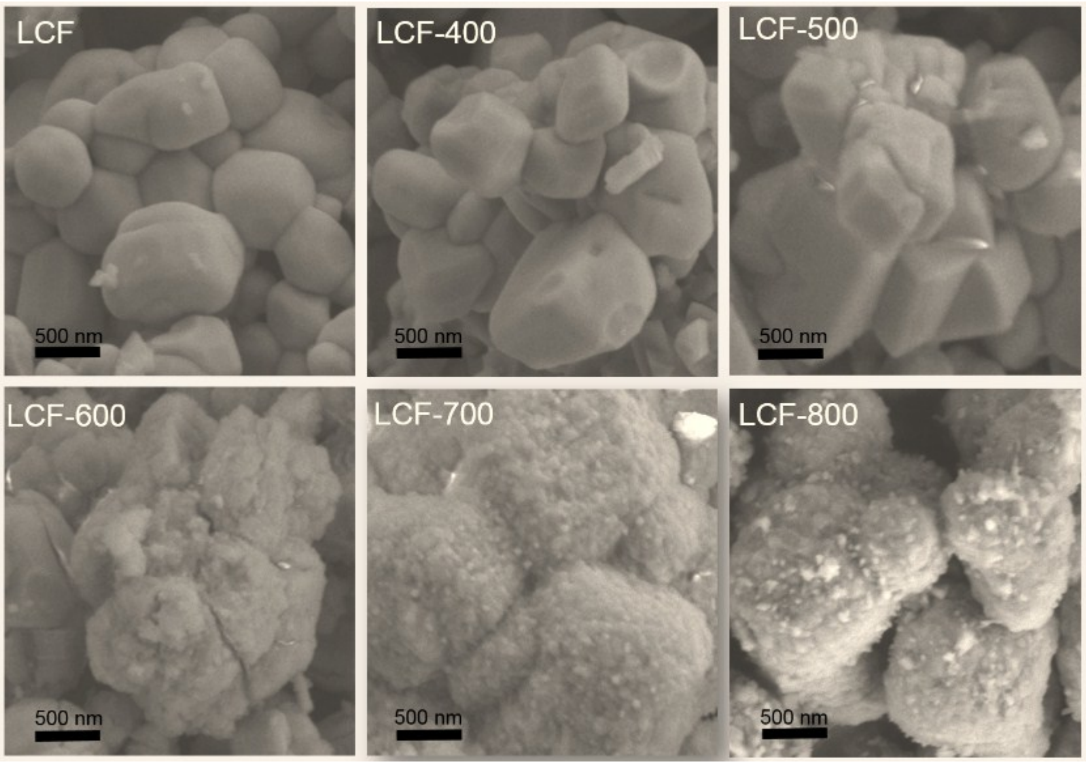

Fig. S4 Scanning electron microscopy (SEM) images of LCF, LCF-400, LCF-500, LCF-600, LCF-700 and LCF-800.

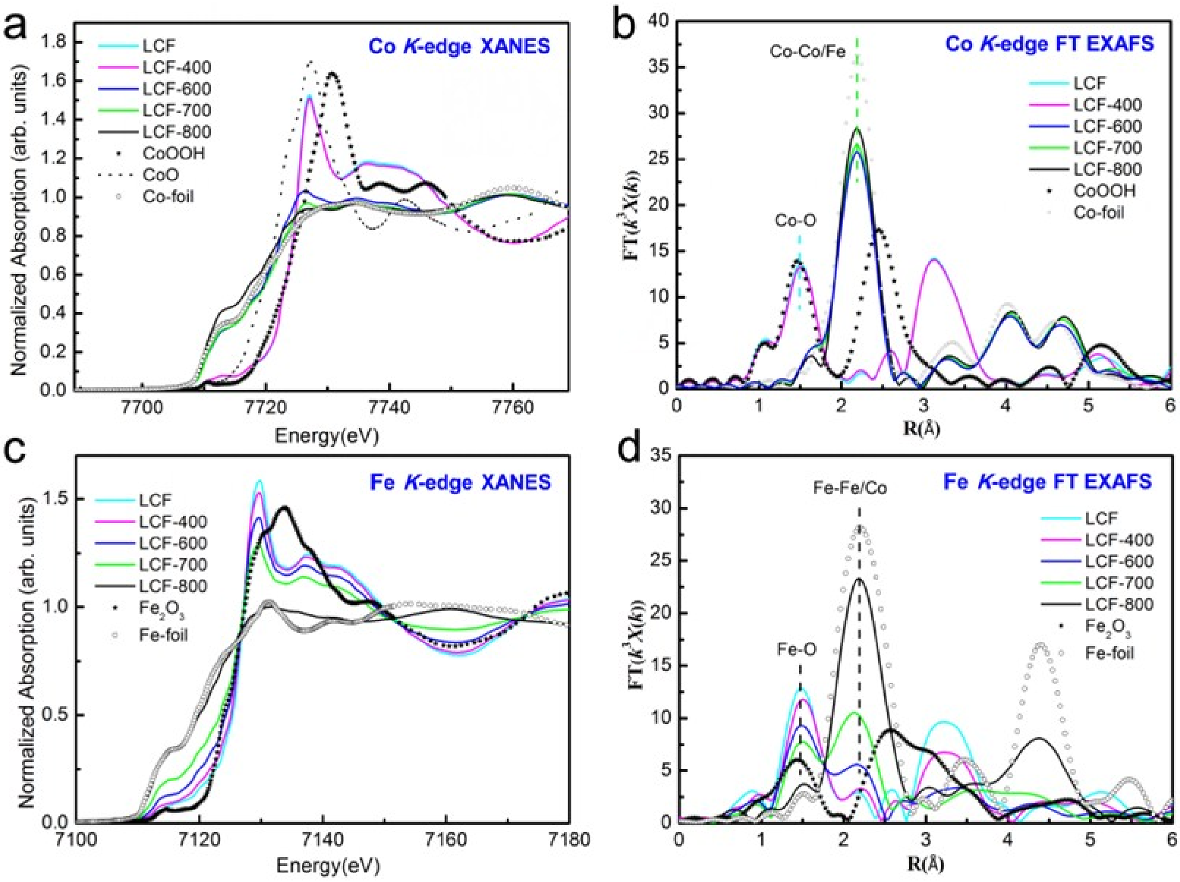

Fig. S5 (a) Co *K*-edge XANES spectra of LCF, LCF-400, LCF-600, LCF-700 and LCF-800 as well as reference samples. (b) Co *K*-edge FT-EXAFS (FT range: 2.5-13.0 Å^{-1}, *k* space in Fig. S27a). (c) Fe *K*-edge XANES spectra of LCF, LCF-400, LCF-600, LCF-700 and LCF-800 as well as reference samples. (d) Fe *K*-edge FT-EXAFS (FT range: 2.5-11.5 Å^{-1}, *k* space in Fig. S27b). The plots are not corrected for phase shift.

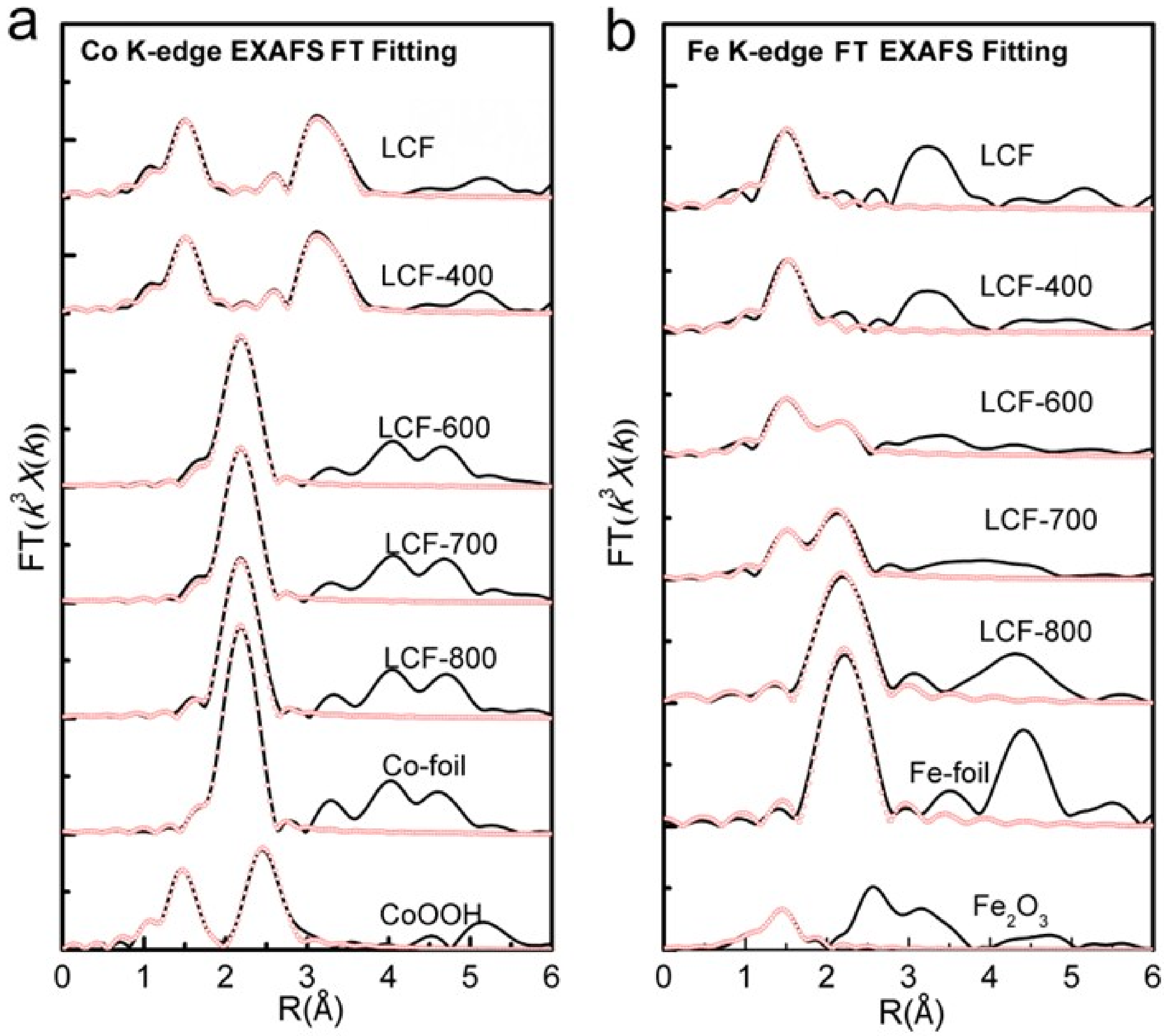

Fig. S6 EXAFS fitting curves for LCF, LCF-400, LCF-600, LCF-700 and LCF-800 as well as reference samples of (a) Co *K*-edge. FT range: 2.5-13.0 Å^{-1}. Fitting range were: Co foil, LCF-600, LCF-700 and LCF-800 (1.5-3.0 Å); CoOOH (1.0-3.0 Å); LCF and LCF-400 (1.0-3.8 Å). (b) Fe *K*-edge. FT range: 2.5-11.5 Å^{-1}. Fitting range were: Fe foil and LCF-800 (1.5-2.8 Å); Fe$_2$O$_3$ (1.0-2.0 Å); LCF, LCF-400, LCF-600 and LCF-700 (1.0-2.6 Å). Co and Fe *K*-edge FT-EXAFS (black lines), the best fitting (red dots). The plots are not corrected for phase shift.

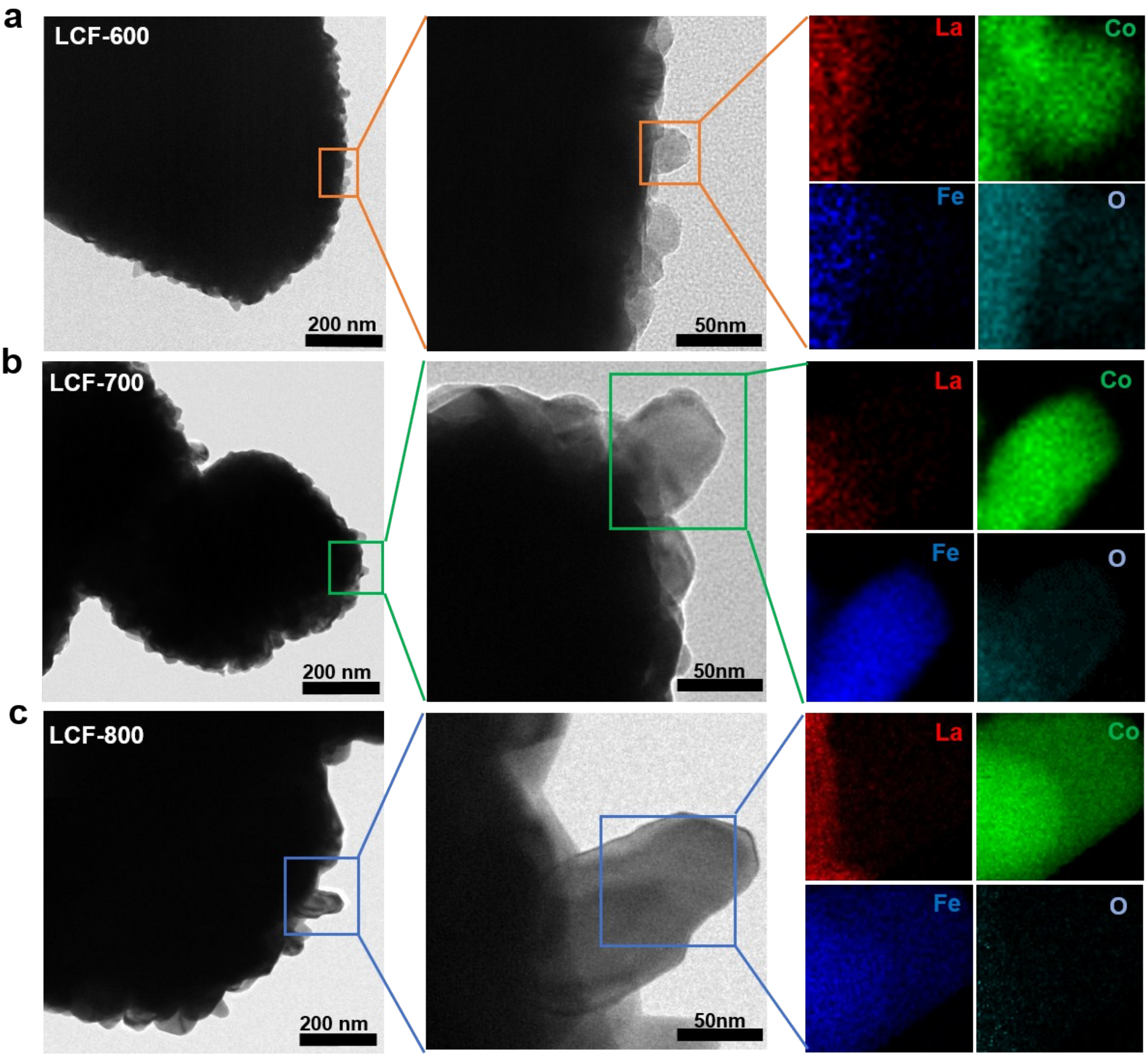

Fig. S7 (a) TEM images and EDX elemental mapping of LCF-600. (b) TEM images and EDX elemental mapping of LCF-700. (c) TEM images and EDX elemental mapping of LCF-800. The size of the metallic nanoparticles in LCF-600 is about 20 nm. These particles are mainly comprised of cobalt while almost no iron signal can be detected. When the LCF catalyst was annealed at 700°C, the size of the metallic nanoparticles is about 30 nm. For LCF-800, the size of the metallic nanoparticles is about 100 nm. Therefore, the size can be finely controlled though the reduction temperature.

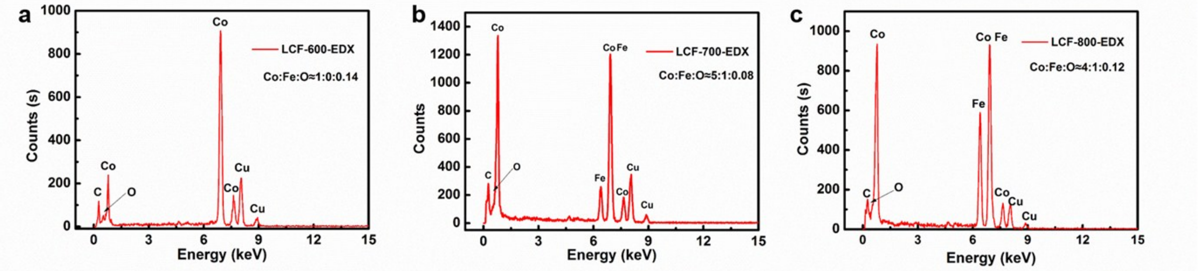

Fig. S8 Energy-dispersive X-ray spectra (EDX) of (a) LCF-600, (b) LCF-700 and (c) LCF-800. LCF-600 is comprised of cobalt while almost no iron signal can be detected. The Co/Fe ratio of LCF-700 is 5:1. For LCF-800, the Co/Fe ratio increases to 4:1. Therefore, Co/Fe ratio increases with increased reduction temperature.

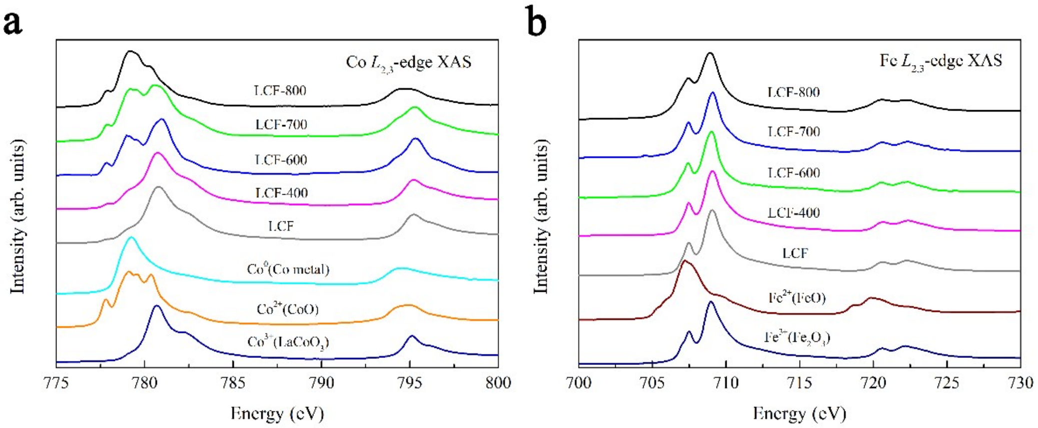

Fig. S9 (a) Co $L_{2,3}$-edge and (b) Fe $L_{2,3}$-edge XAS of LCF, LCF-400, LCF-600, LCF-700 and LCF-800 as well as reference samples. All spectra were measured with the total-electron-yield (TEY) mode with a typical probing depth of 2-5 nm. For LCF and LCF-400, the spectra show the closest resemblance to that of $LaCoO_3$, representing a mainly Co^{3+} valence state. A minor pre-peak at 777.8 eV can be seen and is attributed to the presence of some amount of Co^{2+}, which indicates that some Co^{3+} ions are reduced to Co^{2+} without the appearance of the exsolution structures. When the reduction temperature exceeds 400°C, the spectra changed significantly. The appearances of the characteristic feature of Co^{2+} mentioned above and the peak locating at the similar energy position of the main peak of Co^{3+} indicate that there are Co^{2+} and Co^{3+} ions existing in the surfaces of nanoparticles, besides Co^{0}. Therefore, considering the typical probing depths of 2-5 nm in TEY mode and the fact that Co^{0} have been detected, we can conclude that nanoparticles are covered by ultrathin transition-metal oxides. In contrast, the Fe $L_{2,3}$-edge XAS spectra show Fe^{3+} ions at the surface in all samples.

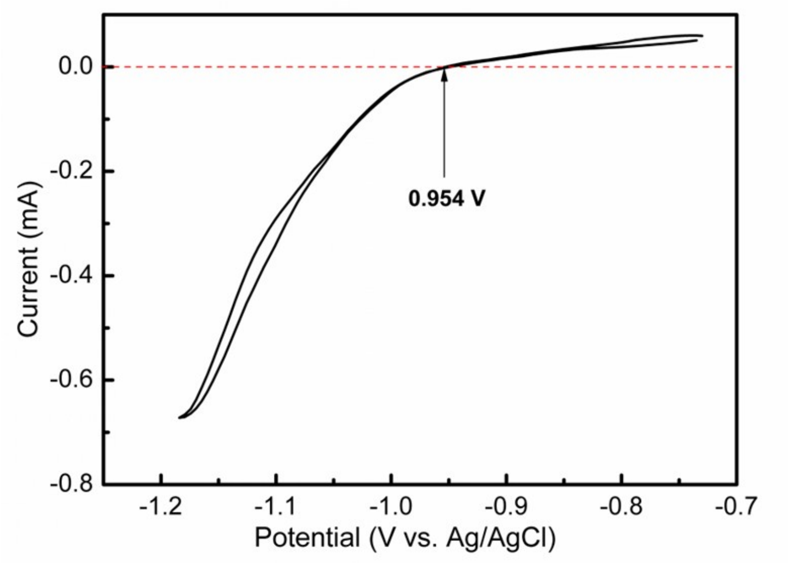

Fig. S10 RHE calibration of the Ag/AgCl reference electrode in 0.1 M KOH. The calibration was performed in the high purity hydrogen saturated electrolyte with a Pt wire as the working electrode. CVs were run at a scan rate of 1 mV s^{-1}, and the average of the two potentials at which the current crossed zero was taken to be the thermodynamic potential for the hydrogen electrode reactions.

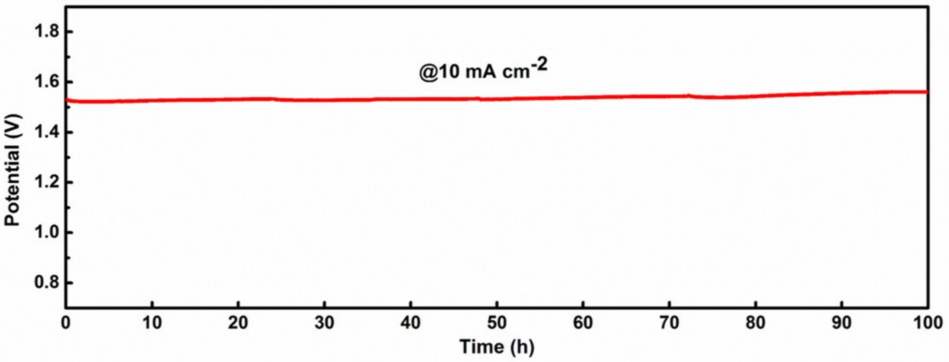

Fig. S11 Chronopotentiometric measurement at *j* = 10 mA cm^{-2} for LCF-700. The long-term test was obtained after the LCF-700 was completely activated and stabilized.

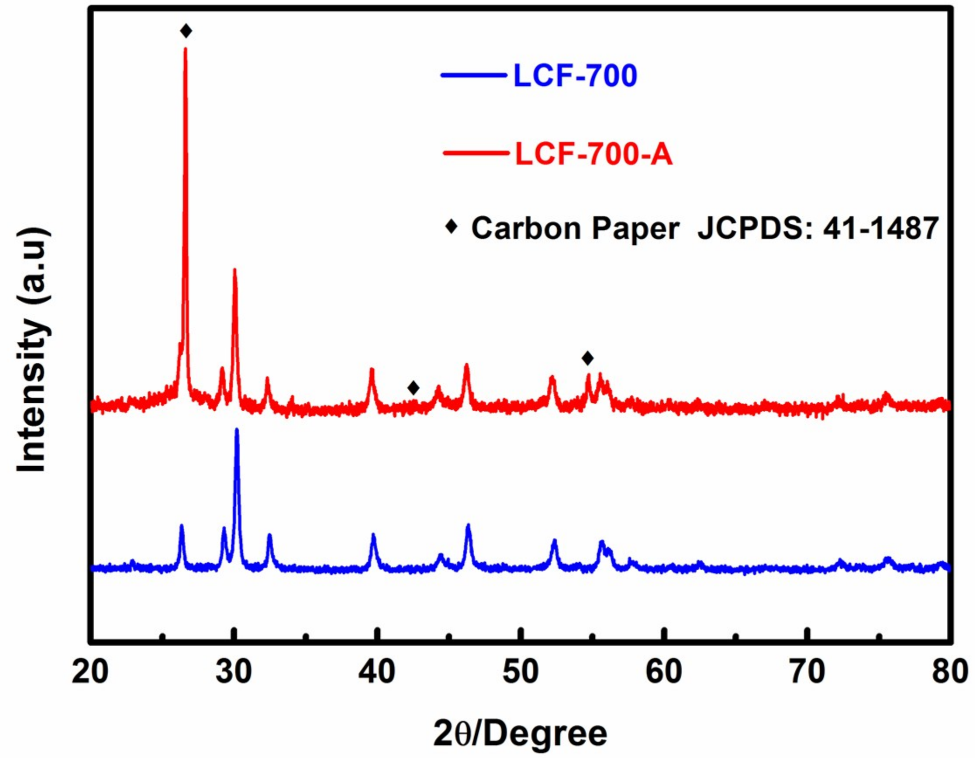

Fig. S12 The XRD patterns of LCF-700 and LCF-700-A. ◆ is the peak of the carbon paper.

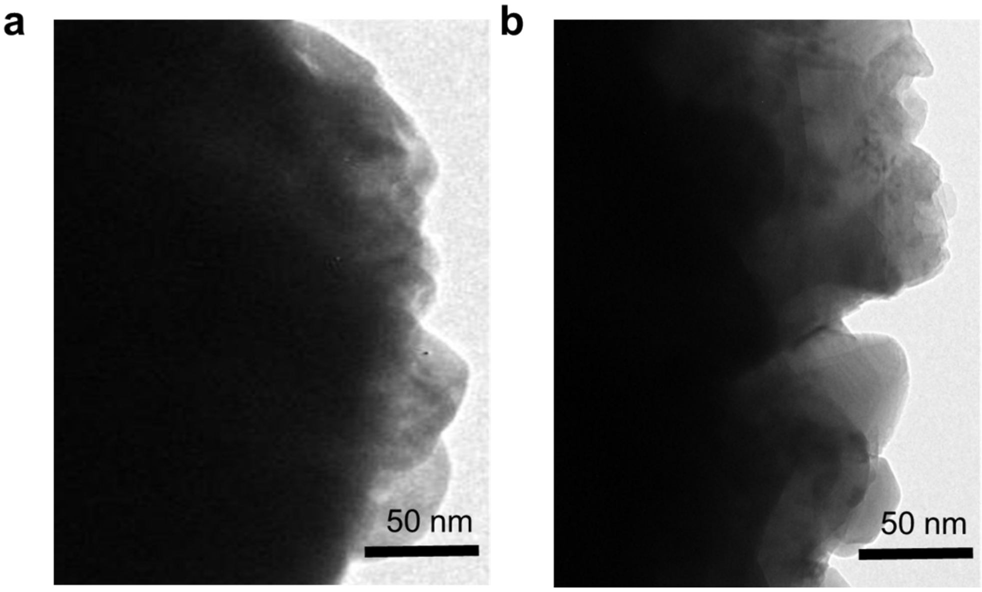

Fig. S13 The TEM images of (a) LCF-700 and (b) LCF-700-A.

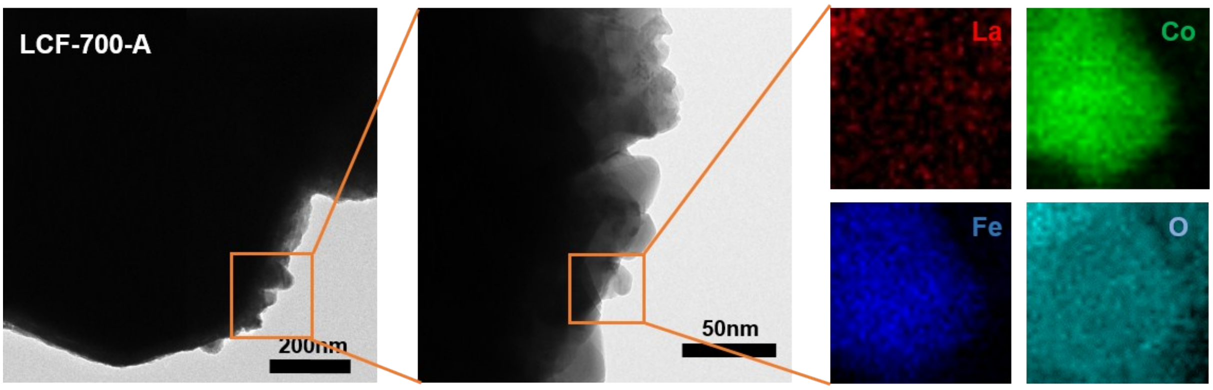

Fig. S14 The TEM images and EDX elemental mapping of LCF-700-A.

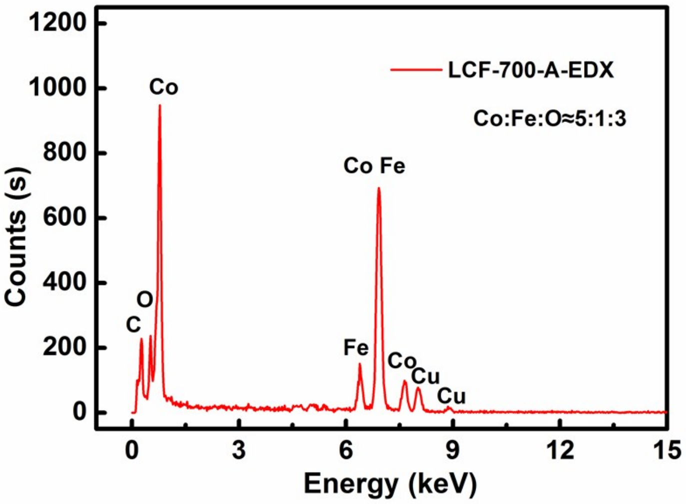

Fig. S15 The EDX spectrum of LCF-700-A.

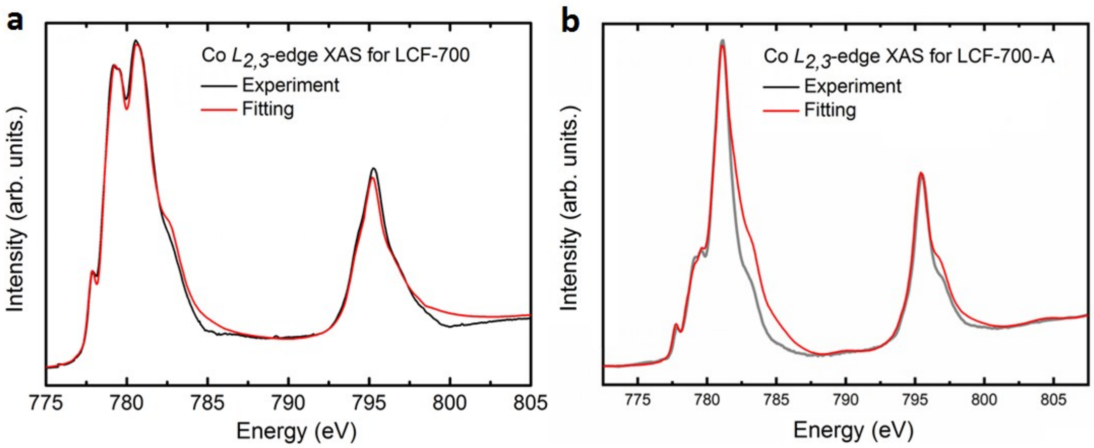

Fig. S16 Fitting of the experimental Co $L_{2,3}$-edge XAS spectra of (a) LCF-700 and (b) LCF-700-A. Data were fitted using a linear combination of the XAS spectra from reference samples (Co metal for Co^0, CoO for Co^{2+}, $LaCoO_3$ for Co^{3+} and $BaCoO_3$ for Co^{4+}). The LCF-700 sample exhibits the content of Co^{2+} and Co^{3+} of 41% and 27%, besides Co^0. It indicates an ultrathin transition-metal oxides surface which arise from the oxidation in the air due to the high surface energy of the as-prepared nanoparticles. By contrast, the LCF-700-A is mainly comprised of Co^{3+} (75%) and also includes some amount of Co^{4+} (15%) and Co^{2+} (10%). This clearly indicates that the thickened oxides surface and the appearance of the Co^{4+} ions which possibly has important contribution to OER activity[S3] on the LCF-700-A sample. All the fitting results are also listed in Table S6.

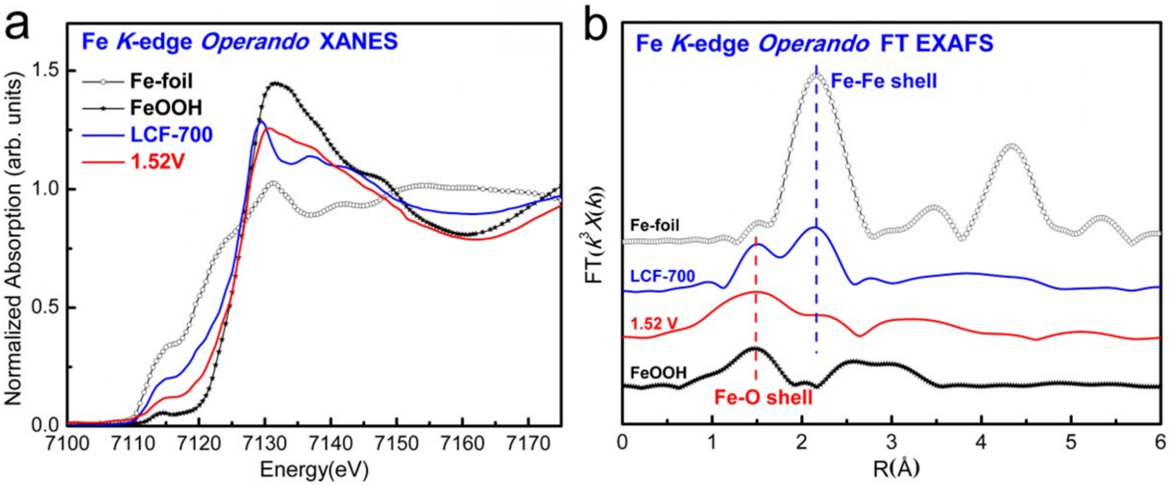

Fig. S17 (a) Fe *K*-edge XANES and (b) FT-EXAFS (FT range: 2.0-10.0 Å^{-1}, Fig. S28) of LCF-700 electrode at 1.52 V vs. RHE in 0.1 M KOH with reference samples. *Operando* XANES and FT-EXAFS at Fe *K*-edge indicate a rise in the Fe oxidation state with the applied potential increasing. The plots are not corrected for phase shift.

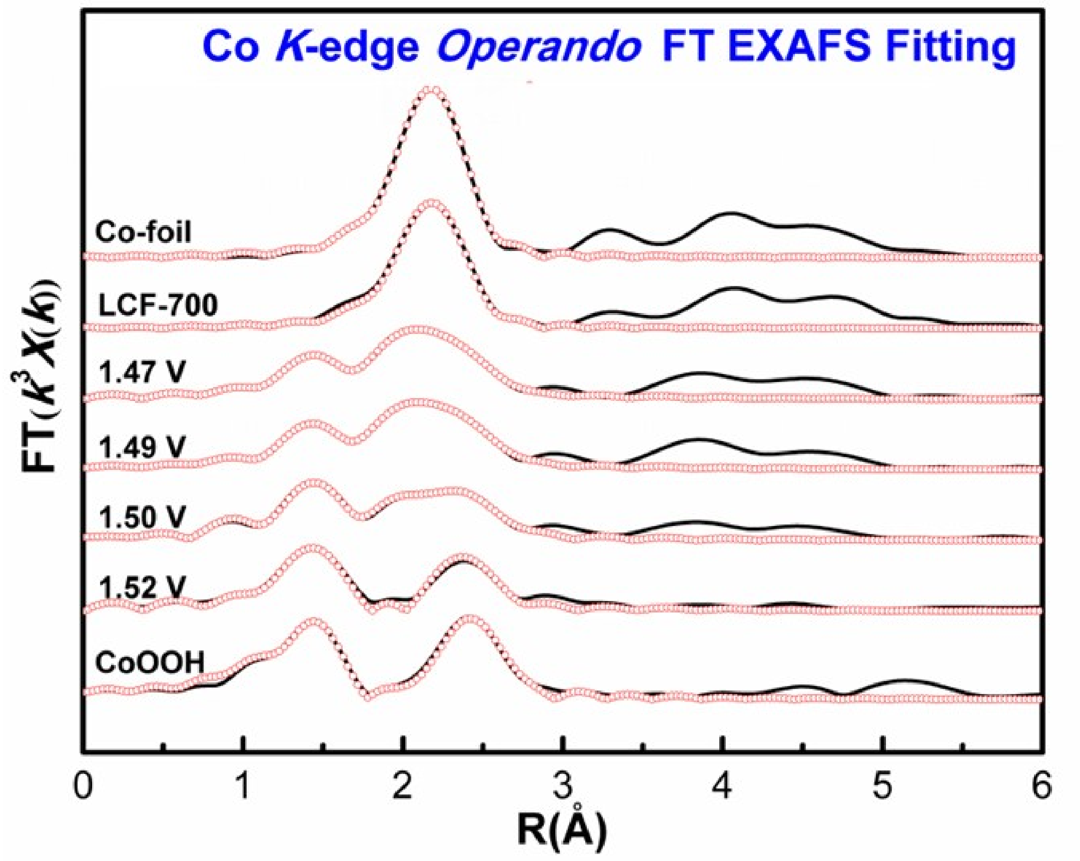

Fig. S18 Co *K*-edge FT-EXAFS fitting curves for LCF-700 electrodes from 1.47 to 1.52 V vs. RHE in 0.1 M KOH (FT range: 2.7-11.0 Å^{-1}, fitting range: 1.0-2.9 Å) as well as reference samples. Co *K*-edge FT-EXAFS (black lines), the best fitting (red dots). The plots are not corrected for phase shift.

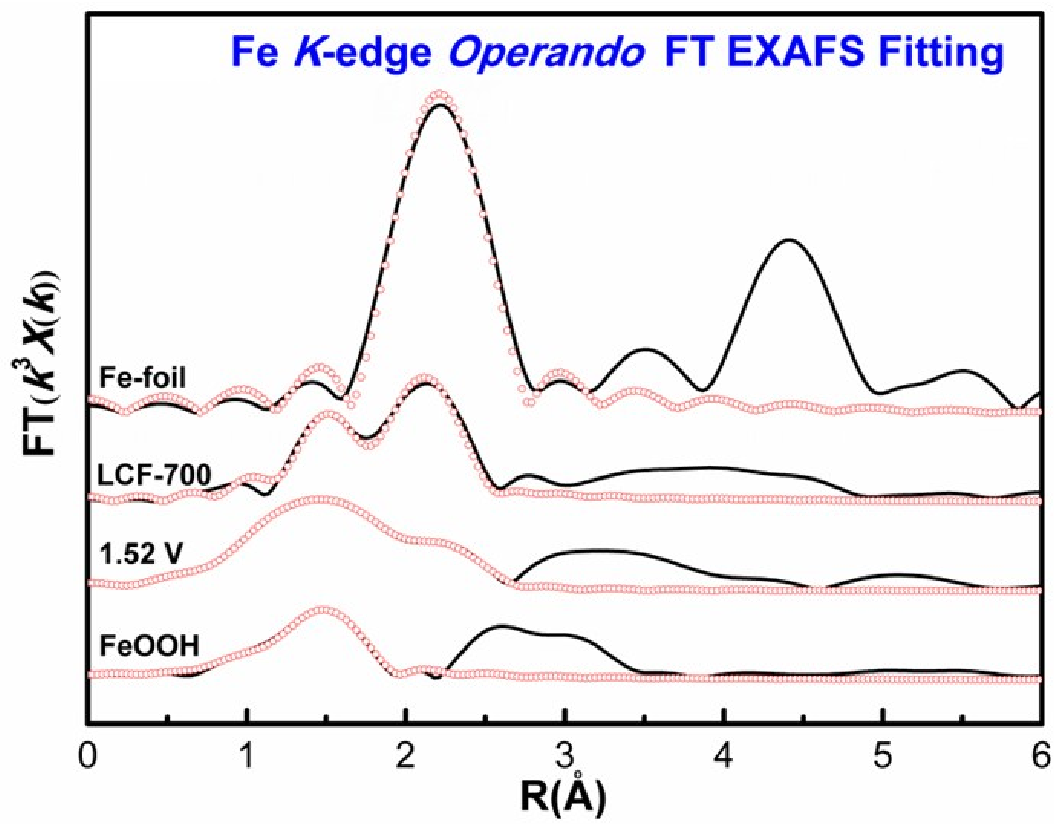

Fig. S19 Fe *K*-edge FT-EXAFS fitting curves for LCF-700 electrodes at 1.52 V vs. RHE in 0.1 M KOH (FT range: 2.0-10.0 Å^{-1}, fitting range: 0.9-2.7 Å) as well as reference samples. Fe *K*-edge FT-EXAFS (black lines), the best fitting (red dots). The plots are not corrected for phase shift.

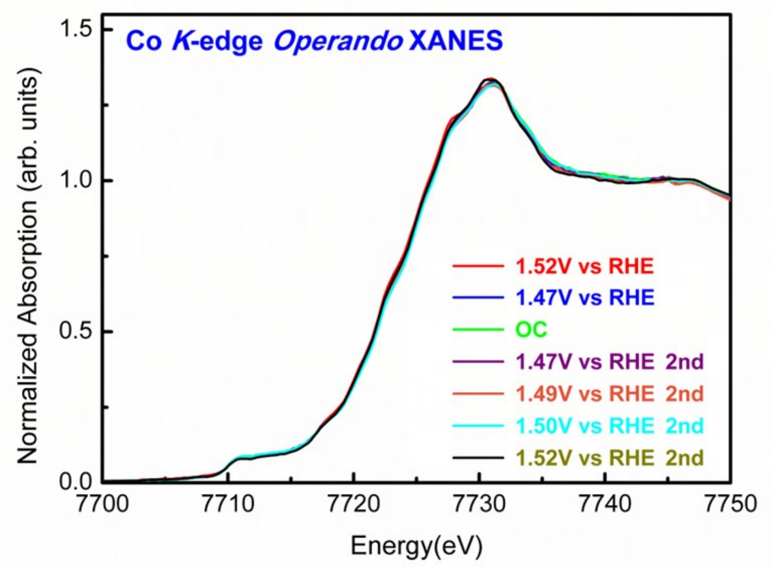

Fig. S20 Co *K*-edge XANES spectra of LCF-700 with the applied potential holding at 1.52 V —1.47 V —open circuit —1.47 V —1.49 V —1.50 V —1.52 V vs. RHE for a decrease-increase process. When the applied potential was reduced to open circuit, the XANES spectrum was nearly unchanged. Even if anodically increasing the applied potential from open circuit to 1.52V again, no significant changes in the Co *K*-edge occur, indicating that the local structure and electronic structure of the LCF-700 didn't change after the catalyst was activated.

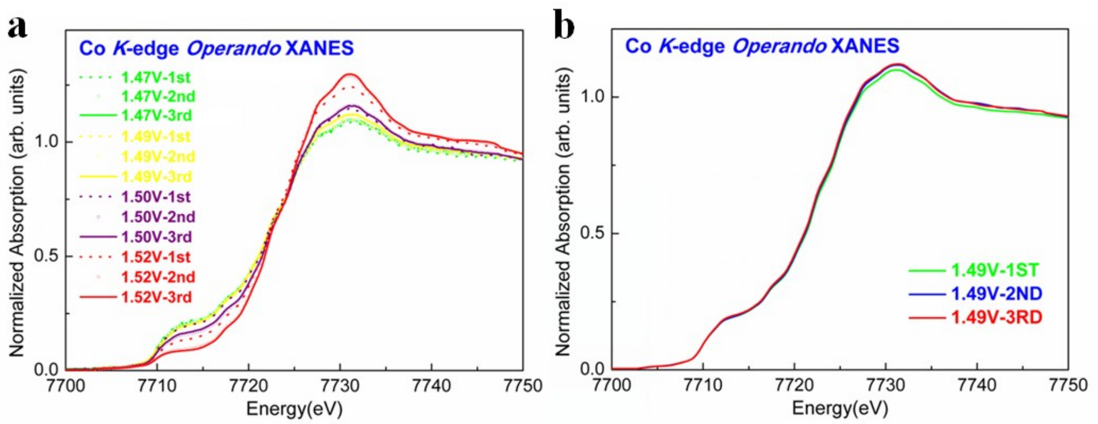

Fig. S21 (a) *Operando* XANES spectra of the LCF-700 electrode at 1.47 V to 1.52 V vs. RHE in 0.1 M KOH. The spectra at each applied potential were measured for three times. (b) Comparison of XANES spectra collected continually for three times at 1.49 V vs. RHE. The measurement time for each spectrum was 5 min. It can be clearly seen that operando XAS have detected a rapid gradual shift of absorption edge towards high energy under current conditions, indicating a rapid transition from metal particles to (oxy)-hydroxide within 10 minutes. *Operando* XAS experiment traced the reconstruction process. It was found that both potential and time have an effect on surface reconstruction, and the potential is the dominant factor from the experimental data.

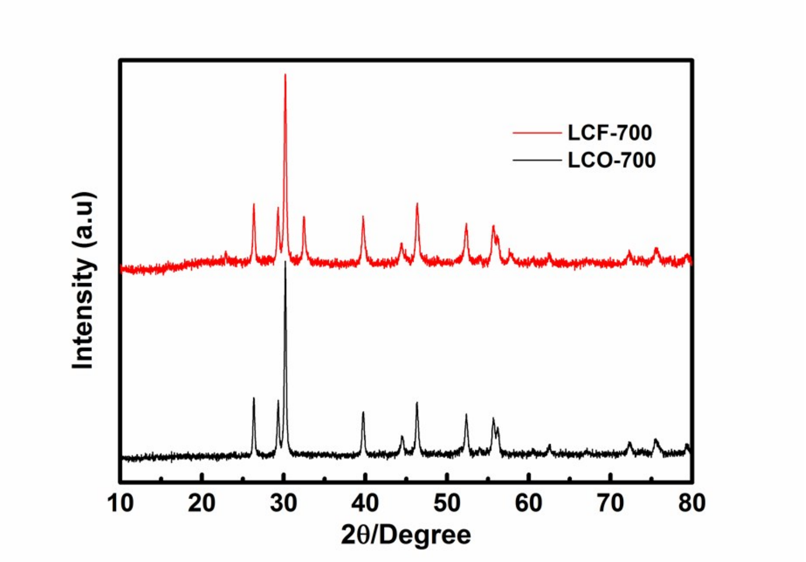

Fig. S22 The XRD patterns of LCF-700 and LCO-700.

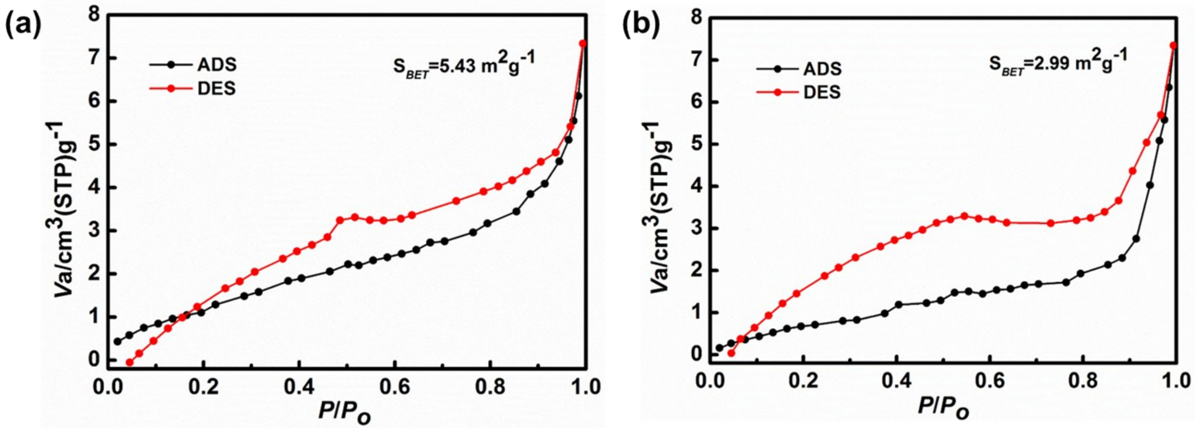

Fig. S23 The BET of (a) LCF-700 and (b) LCO-700.

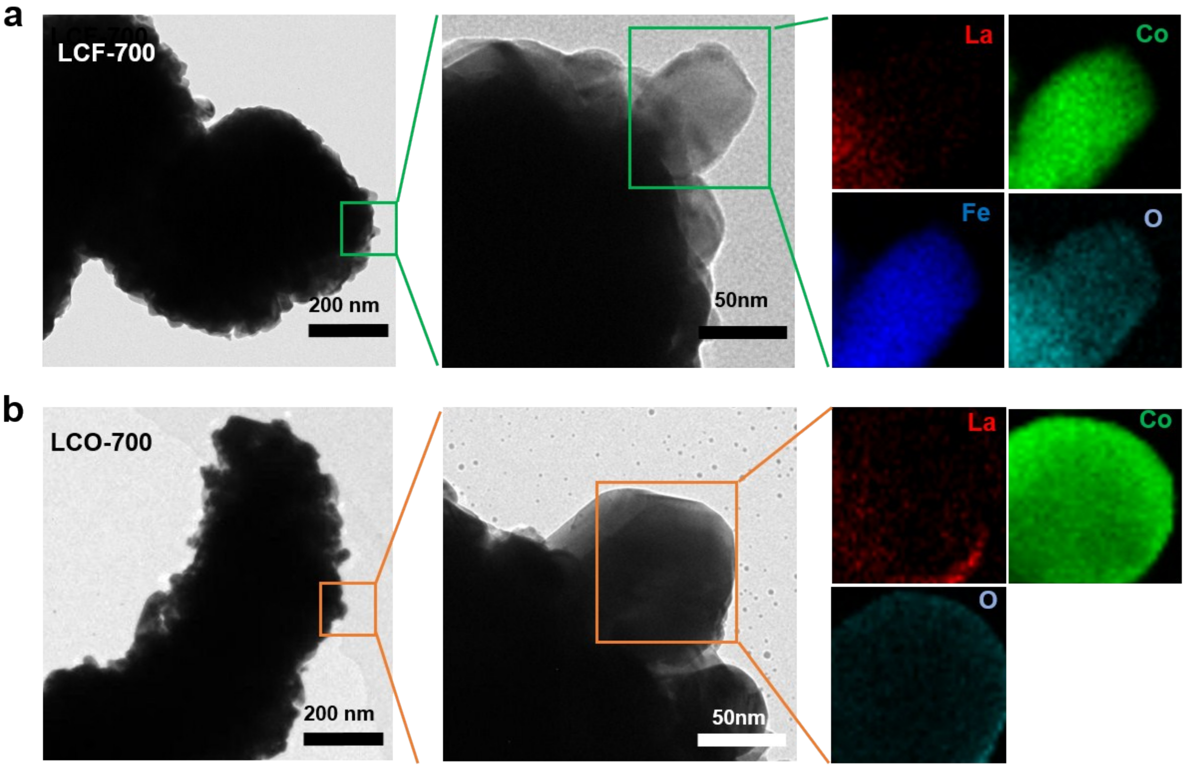

Fig. S24 The TEM images and EDX elemental mapping of (a) LCF-700 and (b) LCO-700.

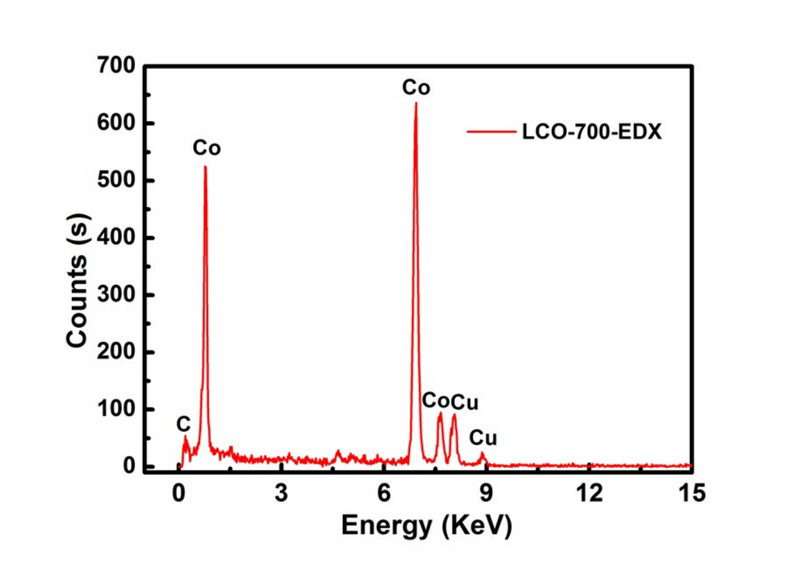

Fig. S25 The EDX spectrum of LCO-700.

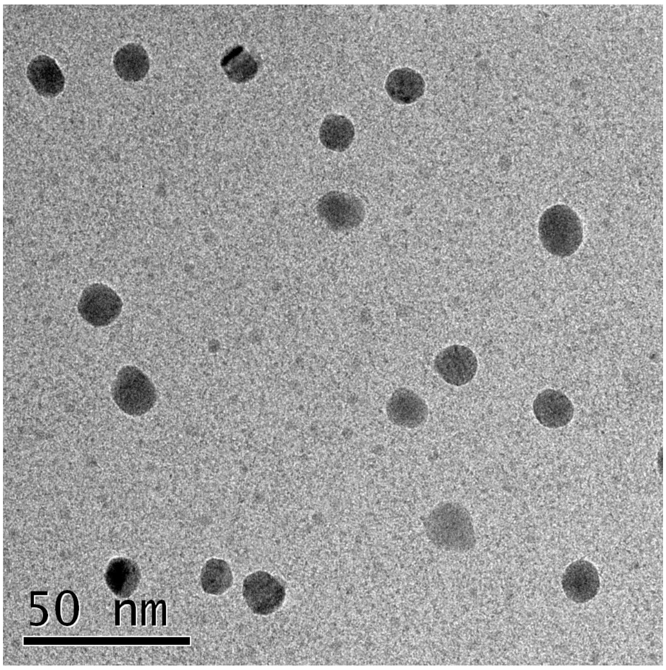

Fig. S26 The TEM image of Co NPs (99.9% metals basis, Alfa Aesar).

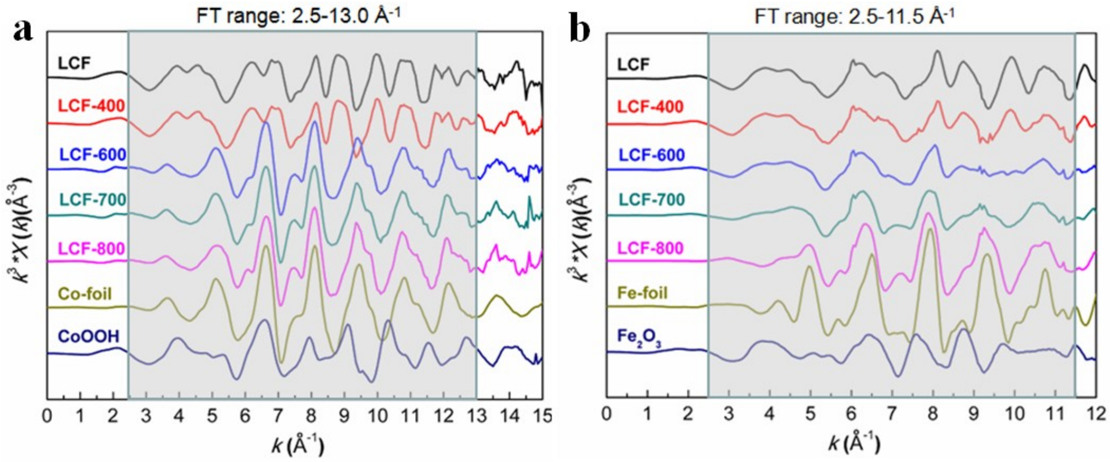

Fig. S27 (a) EXAFS oscillation functions at the Co *K*-edge of LCF, LCF-400, LCF-600, LCF-700 and LCF-800 as well as reference samples. Fourier transformed range: Δk = 2.5-13.0 Å^{-1}. (b) Fe *K*-edge EXAFS. Fourier transformed range: Δk = 2.5-11.5 Å^{-1}.

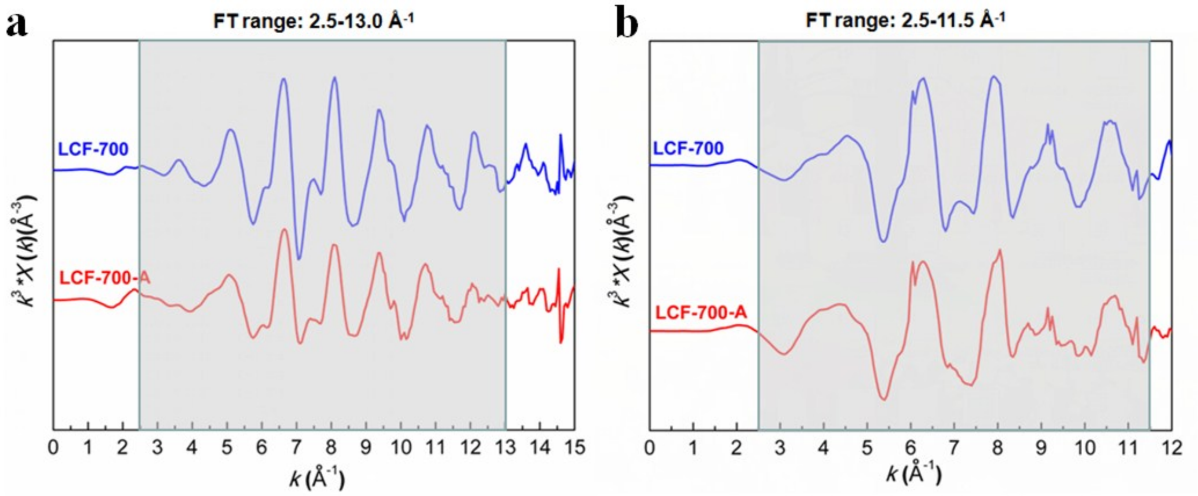

Fig. S28 (a) EXAFS oscillation functions at the Co *K*-edge of LCF-700 and LCF-700-A. Fourier transformed range: Δk = 2.5-13.0 Å^{-1}. (b) Fe K-edge EXAFS. Fourier transformed range: Δk = 2.5-11.5 Å^{-1}.

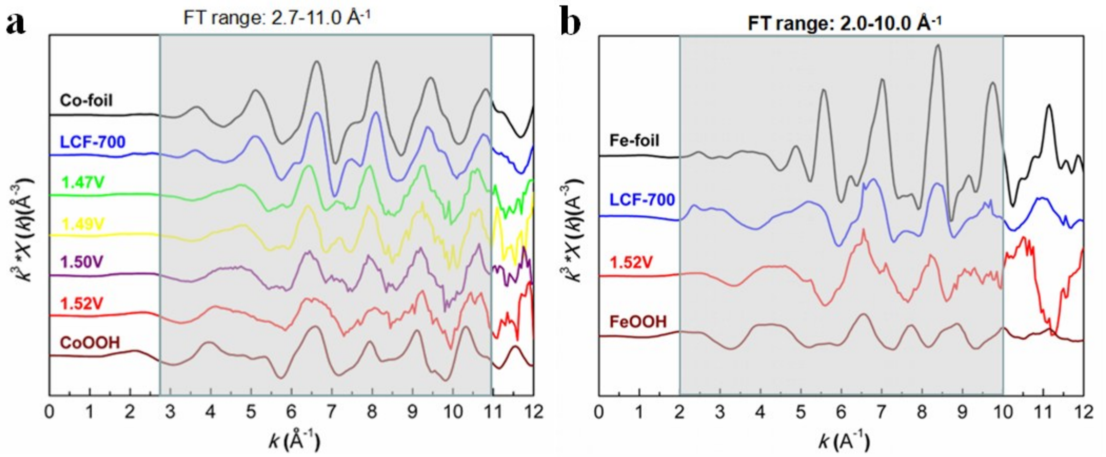

Fig. S29 (a) *Operando* EXAFS oscillation functions at the Co *K*-edge of the LCF-700 electrode at 1.47 to 1.52 V vs. RHE in 0.1 M KOH with reference samples. Fourier transformed range: *Δk* = 2.7-11.0 Å^{-1}. The noise level ratio of the Co *K*-edge *operando* EXAFS increased when *k*>11.0 Å^{-1}. (b) Fe *K*-edge EXAFS. Fourier transformed range: *Δk* = 2.0-10.0 Å^{-1}. The noise level ratio of the Fe *K*-edge *operando* EXAFS increased when *k*>10.0 Å^{-1}.

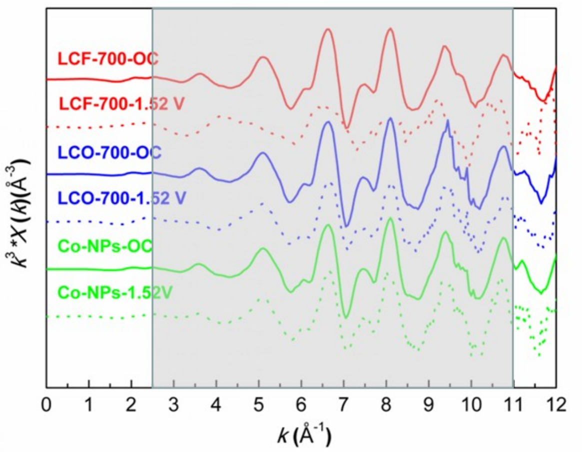

Fig. 30 EXAFS oscillation functions at the Co *K*-edge of LCF-700, LCO-700 and 30nm Co nanoparticles electrodes at open circuit and 1.52 V vs. RHE in 0.1 M KOH. Fourier transformed range: Δ*k* = 2.5-11.0 $Å^{-1}$.

Supporting Tables

Table S1. Structural parameters of LCF, LCF-400, LCF-600, LCF-700, LCF-800 and reference samples extracted from the Co *K*-edge EXAFS fitting (S_0^2=0.73)[a].

Samples	Atomic scatter	No. of atoms (CN)[b]	Interatomic distance (Å)[c]	Debye-Waller factor (10^{-3}×Å^2)[d]	ΔE_0(eV)[e]	R factor
Co-foil	Co-Co	12	2.49±0.03	6.2±0.3	6.8	0.001
CoOOH	Co-O	6	1.91±0.02	2.3±0.3	-6.4	0.013
	Co-Co	6	2.85±0.03	3.3±0.8	-11.1	
LCF-800	Co-Co	9.1±1.8	2.49±0.03	6.0±0.7	7.2	0.010
LCF-700	Co-Co	8.9±1.6	2.49±0.03	6.2±0.5	6.6	0.001
LCF-600	Co-Co	8.8±1.6	2.49±0.03	6.2±0.9	6.8	0.003
LCF-400	Co-O	5.0±1.0	1.93±0.02	2.2±0.3	-2.5	0.016
	Co-La	8.5±1.7	3.33±0.04	7.1±1.4	-5.6	
	Co-Co/Fe	5.3±1.1	3.65±0.04	6.0±2.1	5.7	
LCF	Co-O	5.2±1.1	1.93±0.02	2.3±1.2	-2.5	0.016
	Co-La	8.5±1.7	3.33±0.04	7.0±1.4	-5.5	
	Co-Co/Fe	5.3±1.1	3.65±0.04	6.0±2.0	5.4	

a) S_0^2 was fixed as 0.73 during EXAFS fitting, based on the known structure of Co foil.

b) CN is the coordination number.

c) Interatomic distance is the bond length between Co central atoms and surrounding coordination atoms.

d) Debye-Waller factor is a measure of thermal and static disorder in absorber-scattering distances.

e) ΔE_0 is the difference between the zero kinetic energy value of the sample and that of the theoretical model.

Table S2. Structural parameters of LCF, LCF-400, LCF-600, LCF-700 and LCF-800 with reference samples extracted from the Fe *K*-edge EXAFS fitting (S_0^2=0.70).

Samples	Atomic scatter	N of atoms (CN)	Interatomic distance (Å)	Debye-Waller factor (10^{-3}×Å^2)	ΔE_0(eV)	R factor
Fe-foil	Fe-Fe	12	2.52±0.03	4.4±0.7	9.5	0.006
Fe_2O_3	Fe-O	3	1.92±0.02	3.4±0.9	-7.9	0.006
	Fe-O	3	2.09±0.03	6.7±2.2	-3.2	
LCF-800	Fe- Fe/Co	7.1±1.4	2.50±0.03	3.7±2.7	8.1	0.008
LCF-700	Fe-O	3.6±0.7	1.95±0.02	3.3±2.3	-10.3	0.021
	Fe-Fe/Co	5.2±1.1	2.50±0.03	6.6±0.5	-9.9	
LCF-600	Fe-O	4.6±0.9	1.96±0.02	3.1±0.9	-6.6	0.009
	Fe-Fe/Co	2.5±0.5	2.48±0.03	5.3±1.2	-11.0	
LCF-400	Fe-O	5.6±1.1	1.97±0.02	2.6±0.6	-3.5	0.011
LCF	Fe-O	6.1±1.2	1.96±0.02	2.5±2.9	-5.5	0.014

Table S3. Comparison of OER activities for some state-of-the-art active perovskite catalysts.

Catalysts	Electrolyte	Loading (mg cm^{-2})	Onset Potential (V)	Potential at 10mA cm^{-2} (V)	Surface area (m^{2}g^{-1})	Specific activity (mA cm^{-2})	Substrate	Reference
LCF-700^1	0.1M KOH	0.245	1.47	1.52 VS RHE	5.43	0.75*	GC	This work
$La_{0.95}FeO_3$	0.1M KOH	0.232	1.55	1.64 VS RHE	6.48	0.66*	GC	S4
$SrNb_{0.1}Co_{0.7}Fe_{0.2}O_3$	0.1M KOH	0.232	1.53	1.66 VS RHE	0.25	17.2**	GC	S5
$LaCoO_3$-80nm	0.1M KOH	0.250	1.56	1.72 VS RHE	4.44	0.90*	GC	S6
$SrCoO_{2.7}$^{1}	0.1M KOH	0.0153	~1.55	1.61 VS RHE^a	3.6	28.4***	GC	S7
$PrBaCo_2O_5$^{1}	0.1M KOH	0.250	~1.52	1.58 VS RHE^a	0.35	~20***	GC	S8
$Ba_{0.5}Sr_{0.5}Co_{0.8}Fe_{0.2}O_3$^{1}	0.1M KOH	0.250	~1.56	~1.58 VS RHE^a	0.2	~40***	GC	S9
$La_{0.7}(Ba_{0.5}Sr_{0.5})_{0.3}Co_{0.8}Fe_{0.2}O_{3-\delta}$	0.1M KOH	0.639	~1.50	~1.60 VS RHE	21.9	0.071*	GC	S10
Amorphous $Ba_{0.5}Sr_{0.5}Co_{0.8}Fe_{0.2}O_{3-\delta}$ nano film	1 M KOH	0.1548	1.46	~1.52 VS RHE	-	-	NF	S11
Co_3O_4/N-rmGO	1 M KOH	0.240	-	1.54 VS RHE	-	-	NF	S12
NiFe-LDH/CNT	0.1M KOH	0.200	1.50	1.538 VS RHE	-	-	GC	S13
NiFe-NS^1	1 M KOH	0.070	1.491	1.532 VS RHE	-	-	GC	S14
γ-CoOOH NS	1 M KOH	0.150	1.47	1.53 VS RHE	-	-	GC	S15
NiFe/NF	0.1 M KOH	-	1.44	1.47 VS RHE	-	-	NF	S16
CoFeOx/Ni foam	1 M KOH	0.020	-	1.50 VS RHE	-	-	NF	S17
FeOOH/Co/FeOOH HNTAs-NF	1 M NaOH	-	1.45	1.47 VS RHE	-	-	NF	S18
CoNi(OH)x	1 M KOH	0.720	1.48	1.51 VS RHE	-	-	Cu-foil	S19
NiCo-LDH-NA	1 M KOH	0.800	-	1.537 VS RHE	-	-	CFP	S20
Ni-P	1 M KOH	0.200	1.48	1.53 VS RHE	35	0.14*	GC	S21
Ni_3Se_2	0.3 M KOH	0.0614	1.45	1.54 VS RHE	-	-	GC	S22
CoFe-LDH	1 M KOH	0.200	1.53	1.63 VS RHE	-	-	ITO	S23
CoSn-T1	1 M KOH	0.283	-	1.543 VS RHE	-	-	GC	S24
NF/oLCFO-Ar	0.1M KOH	1.07	-	1.58 VS RHE	-	-	NF	S25
NiFe LDH	1 M KOH	0.05	-	1.49 VS RHE	-	-	GC	S26
Fe-CoOOH/G	1 M KOH	0.200	1.51	1.56 VS RHE	238	0.021*	GC	S27
$W_{0.5}Co_{0.4}Fe_{0.1}$/NF	1 M KOH	-	-	1.48 VS RHE	-	-	NF	S28

CoFe LDHs nanosheets[1]	1 M KOH	0.204	1.497	1.551 VS RHE	32.7	0.15*	GC	S29
$NaCo_{0.8}Fe_{0.2}O_2$	1 M KOH	0.130	-	1.56 VS RHE	-	-	GC	S30
Au/NiFe LDH	1 M KOH	200	-	1.467 VS RHE	-	-	Ti mesh	S31
Ni-Fe LDH hollow nanoprisms	1 M KOH	0.160	-	1.51 VS RHE	250	0.025*	GC	S32

NS = Nano Sheet, rmGO = reduced Mildly Oxidized Graphene Oxide, NF = Ni Foam, G = Graphene, CNT = Carbon Nanotube, NA = Nanoarrays, HNTAs = Hybrid Nanotube Arrays,

[1] Onset potential at about 1 mA cm^{-2},

[a] Calculated from the specific activity,

The value is Calculated from the specific activity = j / (10×m×S_{BET}),

* Specific activity calculated at the overpotential (η) when j = 10 mA cm^{-2}.

** Specific activity at η=0.5 V

*** Specific activity at η=0.4 V

Substrate: GC = Glass Carbon, CFP = Carbon Fiber Papers.

Table S4. Structural parameters of LCF-700 electrodes at 1.47 to 1.52 V vs. RHE in 0.1 M KOH with reference samples extracted from the Co *K*-edge EXAFS fitting (S_0^2=0.73).

Samples	Atomic scatter	No. of atoms (CN)	Interatomic distance (Å)	Debye-Waller factor (10^{-3}×Å^2)	ΔE$_0$(eV)	R factor
Co-foil	Co-Co	12	2.49±0.03	6.2±0.3	6.8	0.001
CoOOH	Co-O	6	1.91±0.02	2.3±0.3	-6.4	0.013
	Co-Co	6	2.85±0.03	3.3±0.8	-11.1	
LCF-700	Co-Co	8.9±1.6	2.49±0.03	6.2±0.5	6.6	0.001
1.47 V	Co-O	2.4±0.5	1.87±0.02	2.4±0.6	-7.6	0.001
	Co-Co/Fe	5.1±1.0	2.48±0.03	5.2±1.3	-7.6	
	Co-Co/Fe	2.1±0.4	2.82±0.03	3.6±0.7	-7.6	
1.49 V	Co-O	2.6±0.7	1.88±0.02	2.5±0.4	-6.9	0.001
	Co-Co/Fe	4.9±0.7	2.49±0.03	4.9±1.3	-6.9	
	Co-Co/Fe	2.2±0.5	2.82±0.03	3.6±0.7	-6.9	
1.50 V	Co-O	3.4±0.7	1.89±0.02	2.7±0.5	-4.2	0.004
	Co-Co/Fe	3.5±0.7	2.50±0.03	5.2±1.1	-4.2	
	Co-Co/Fe	2.3±0.5	2.83±0.03	3.1±0.9	-4.2	
1.52 V	Co-O	4.9±1.0	1.88±0.02	3.0±0.7	-7.5	0.020
	Co-Co/Fe	3.6±0.7	2.81±0.03	3.5±1.1	-12.5	

Table S5. Structural parameters of LCF-700 electrodes at 1.52 V vs. RHE in 0.1 M KOH with reference samples extracted from the Fe *K*-edge EXAFS fitting (S_0^2=0.70).

Samples	Atomic scatter	N of atoms (CN)	Interatomic distance (Å)	Debye-Waller factor (10^{-3}×Å^2)	ΔE_0(eV)	R factor
Fe-foil	Fe-Fe	12	2.52±0.03	4.4±0.7	9.5	0.006
FeOOH	Fe-O	6	1.99±0.02	11.0±1.7	-4.3	0.002
LCF-700	Fe-O	3.6±0.7	1.95±0.02	3.3±2.3	-10.3	0.021
	Fe-Fe/Co	5.2±1.1	2.50±0.03	6.6±0.5	-9.9	
1.52 V	Fe-O	5.2±1.1	1.97±0.02	3.6±0.7	-3.7	0.002
	Fe-Fe	2.1±0.4	2.53±0.03	5.6±1.8	-1.1	

Table S6. Fitting results of Co-$L_{2,3}$ XAS spectra of LCF-700 and LCF-700-A.

	Co^0 (%)	Co^{2+} (%)	Co^{3+} (%)	Co^{4+} (%)
LCF-700	32	41	27	0
LCF-700-A	0	10	75	15

References

(S1) H. J. Lin, Y. Y. Chin, Z. Hu, G. J. Shu, F. C. Chou, H. Ohta, K. Yoshimura, S. Hébert, A. Maignan, A. Tanaka, L. H. Tjeng and C. T. Chen, *Phys. Rev. B.*, 2010, **81**, 115138.

(S2) H. Ohta, K. Yoshimura, Z. Hu, Y. Y. Chin, H. J. Lin, H. H. Hsieh, C. T. Chen and L. H. Tjeng, *Phys. Rev. Lett.*, 2011, **107**, 066404.

(S3) C. N. Brodsky, R. G. Hadt, D. Hayes, B. J. Reinhart, N. Li, L. X. Chen and D. G. Nocera, *Proc. Natl. Acad. Sci.*, 2017, **114**, 3855-3860.

(S4) Y. Zhu, W. Zhou, J. Yu, Y. Chen, M. Liu and Z. Shao, *Chem. Mater.*, 2016, **28**, 1691-1697.

(S5) Y. Zhu, W. Zhou, Z. G. Chen, Y. Chen, C. Su, M. O. Tade and Z. Shao, *Angew. Chem. Int. Ed.,* 2015, **54**, 3897-3901.

(S6) S. Zhou, X. Miao, X. Zhao, C. Ma, Y. Qiu, Z. Hu, J. Zhao, L. Shi and J. Zeng, *Nat. Commun*., 2016, **7**, 11510.

(S7) J. T. Mefford, X. Rong, A. M. Abakumov, W. G. Hardin, S. Dai, A. M. Kolpak, K. P. Johnston and K. J. Stevenson, *Nat.Commun*., 2016, **7**, 11053.

(S8) A. Grimaud, K. J. May, C. E. Carlton, Y. L. Lee, M. Risch, W. T. Hong, J. Zhou and Y. Shao-Horn, *Nat. Commun*., 2013, **4**, 2439.

(S9) J. Suntivich, K. J. May, H. A. Gasteiger, J. B. Goodenough and Y. Shao-Horn, *Science*, 2011, *334*, 1383-1385.

(S10) J.-I. Jung, M. Risch, S. Park, M. G. Kim, G. Nam, H.-Y. Jeong, Y. Shao-Horn and J. Cho, *Energ. Environ. Sci.*, 2016, **9**, 176-183.

(S11) G. Chen, W. Zhou, D. Q. Guan, J. Sunarso, Y. P. Zhu, X. F. Hu, W. Zhang and Z. P. Shao, *Sci. Adv*., 2017, **3**, e1603206.

(S12) Y. Liang, Y. Li, H. Wang, J. Zhou, J. Wang, T. Regier and H. Dai, *Nat. Mater*., 2011, **10**, 780-786.

(S13) M. Gong, Y. Li, H. Wang, Y. Liang, J. Z. Wu, J. Zhou, J. Wang, T. Regier, F. Wei and H. Dai, *J. Am. Chem. Soc.*, 2013, **135**, 8452-8455.

(S14) F. Song and X. Hu, *Nat. Commun*., 2014, **5**, 4477.

(S15) J. Huang, J. Chen, T. Yao, J. He, S. Jiang, Z. Sun, Q. Liu, W. Cheng, F. Hu, Y. Jiang, Z. Pan and S. Wei, *Angew. Chem. Int .Ed*, 2015, **54**, 8722-8727.

(S16) X. Lu and C. Zhao, *Nat. Commun*., 2015, **6**, 6616.

(S17) C. G. Morales-Guio, L. Liardet and X. Hu, *J. Am. Chem. Soc.*, 2016, **138**, 8946-8957.

(S18) J. X. Feng, H. Xu, Y. T. Dong, S. H. Ye, Y. X. Tong and G. R. Li, *Angew. Chem. Int. Ed*, 2016, **55**, 3694-3698.

(S19) S. Li, Y. Wang, S. Peng, L. Zhang, A. M. Al-Enizi, H. Zhang, X. Sun and G. Zheng, *Adv. Energy. Mater.*, 2016, **6**, 1501661.

(S20) C. Yu, Z. Liu, X. Han, H. Huang, C. Zhao, J. Yang and J. Qiu, *Carbon*, 2016, **110**, 1-7.

(S21) X.-Y. Yu, Y. Feng, B. Guan, X. W. Lou and U. Paik, *Energy. Environ. Sci.*, 2016, **9**, 1246-1250.

(S22) A. T. Swesi, J. Masud and M. Nath, *Energy. Environ. Sci*., 2016, **9**, 1771-1782.

(S23) L. Feng, A. Li, Y. Li, J. Liu, L. Wang, L. Huang, Y. Wang and X. Ge, *ChemPlusChem*, 2017, **82**, 483-488.

(S24) F. Song, K. Schenk and X. Hu, *Energy. Environ. Sci*., 2016, **9**, 473-477.

(S25) B. Q. Li, C. Tang, H. F. Wang, X. L. Zhu and Q. Zhang, *Sci. Adv.*, 2016, **2**, e1600495.

(S26) R. Chen, G. Sun, C. Yang, L. Zhang, J. Miao, H. Tao, H. Yang, J. Chen, P. Chen and B. Liu, *Nanoscale Horizons*, 2016, **1**, 156-160.

(S27) X. Han, C. Yu, S. Zhou, C. Zhao, H. Huang, J. Yang, Z. Liu, J. Zhao and J. Qiu, *Adv. Energy. Mater*., 2017, **7**, 1602148.

(S28) Y. Pi, Q. Shao, P. Wang, F. Lv, S. Guo, J. Guo and X. Huang, *Angew. Chem. Int. Ed.*, 2017, **129**, 4573.

(S29) Y. Wang, Y. Zhang, Z. Liu, C. Xie, S. Feng, D. Liu, M. Shao and S. Wang, *Angew. Chem. Int. Ed.*, 2017, **56**, 5867.

(S30) B. Weng, F. Xu, C. Wang, W. Meng, C. R. Grice and Y. Yan, *Energ. Environ. Sci*., 2017, **10**, 121-128.

(S31) J. Zhang, J. Liu, L. Xi, Y. Yu, N. Chen, S. Sun, W. Wang, K. M. Lange and B. Zhang, *J. Am. Chem. Soc.*, 2018, **140**, 3876-3879.

(S32) L. Yu, J. F. Yang, B. Y. Guan, Y. Lu and X. W. D. Lou, *Angew. Chem. Int. Ed*., 2018, **57**, 172-176.